Haueisen, Jens; Dietzel, Alexander; Liehr, Mario; Weiser, Thomas; Elsarnagawy, Tarek; Bellemann, Matthias E.:

Bioelectric and biomagnetic measurements are differentially sensitive to spiral currents

Zuerst erschienen in:	Biomedizinische Technik = Biomedical Engineering. - Berlin [u.a.] : de Gruyter. - 56 (2011), 5, p. 283-289.
Erstveröffentlichung:	2011-10-12
ISSN (online):	1862-278X
ISSN (print):	0013-5585
DOI:	10.1515/BMT.2011.104
[*Zuletzt gesehen:*	2019-08-15]

Biomed Tech 2011; 56:283–289 © 2011 by Walter de Gruyter • Berlin • Boston. DOI 10.1515/BMT.2011.104

Bioelectric and biomagnetic measurements are differentially sensitive to spiral currents

Jens Haueisen[1–3,*], Alexander Dietzel[1], Mario Liehr[2], Thomas Weiser[4], Tarek Elsarnagawy[3] and Matthias E. Bellemann[4]

[1] Institute for Biomedical Engineering and Informatics, Ilmenau University of Technology, Germany
[2] Biomagnetic Center, Department of Neurology, University Hospital Jena, Germany
[3] Department of Applied Medical Sciences, King Saud University, Riyadh, Saudi Arabia
[4] Department of Medical Engineering and Biotechnology, University of Applied Sciences, Jena, Germany

Abstract

Observations indicate that different information is contained in electrocardiograms and magnetocardiograms in both patients and healthy volunteers. Closed loop currents could explain this phenomenon. We hypothesized that open loops, such as the spirally shaped currents in the heart, also contribute to these differences. We modeled two types of open spiral-shaped loops, based on the heart geometry, using 12 artificial current dipoles in a physical torso phantom. The electric potentials and magnetic fields were measured simultaneously with increasing numbers of active dipoles in the spiral source geometries. We found a continuous increase in the measured amplitudes of the magnetic fields, up to a plateau value when 10 active dipoles were enabled. For the electric potentials, we found that the amplitudes increased when up to six or eight active dipoles had been enabled, and then decreased thereafter. We conclude that open loop currents also contribute to the experimentally observed differences in magnetocardiograms and electrocardiograms in both patients and healthy volunteers. Combined bioelectric and biomagnetic measurements should provide greater insight into heart activity than do single modality measurements.

Keywords: electrocardiography; ischemia; magnetocardiography; vortex currents.

Introduction

Bioelectric surface potentials and biomagnetic fields measured outside the body can non-invasively provide information about the electrically active tissues in the human body (for a recent review, see e.g., [18]). Electrocardiography (ECG) and magnetocardiography (MCG) are two modalities used to assess the electric heart function. Although the underlying sources are the same for bioelectric potentials and biomagnetic fields, different information can be contained in the two modalities (e.g., [10]).

Experimental observations in patients have indicated divergent ECG and MCG findings during both rest [12, 13, 15, 21] and exercise (e.g., [16]). This different information can also be seen in healthy volunteers during exercise (e.g., [4, 19]).

Closed loop currents, also referred to as vortex currents, have long been discussed as possible sources of the different information available in magnetocardiograms and electrocardiograms [2, 17, 23]. According to the theoretical concept, closed loop currents produce biomagnetic fields but not bioelectric potentials. Previously, we demonstrated that both active and passive vortex currents can be produced experimentally in a torso phantom and our experimental results were in agreement with theoretical predictions [5, 14].

Besides the closed loop currents in the heart, open loop currents can also arise from the spiral arrangement of muscle fibers. Based on a theoretical analysis of multipole expansions, Irimia and colleagues [10] argued that asymmetries occur in spiral-like structures and electrically silent magnetic fields should be prominent. Consequently, the question arises how realistically shaped, spiral open loop currents contribute to ECG and MCG and thus potentially contribute to the experimentally observed differences in them. Therefore, the aim of this study was to analyze the influence of spiral open loop currents on electric and magnetic signals. To do this, we simultaneously recorded the electrical and magnetic data produced by dipole setups in a human torso phantom.

Materials and methods

Phantom setup

We used a realistically shaped torso phantom, built from resin with glass fibers [20]. One hundred and thirty-eight Ag/AgCl electrodes for the acquisition of electric data were embedded in the surface of the phantom (Figure 1A). The phantom was filled with saline solution to reproduce the physiological conductivity inside the torso phantom (conductivity of 0.335 S/m) [6].

We produced two different spirally shaped source setups. The first setup consisted of 12 dipoles forming a planar spiral, and the second setup consisted of 12 dipoles forming a spatially extended spiral (Figure 1B, C). Figure 1C shows

*Corresponding author: University-Prof. Dr Ing. habil. Jens Haueisen, Ilmenau University of Technology, Institute for Biomedical Engineering and Informatics, PO Box 100565, 98684 Ilmenau, Germany
Phone: +49-3677-69-2861
Fax: +49-3677-69-1311
E-mail: jens.haueisen@tu-ilmenau.de

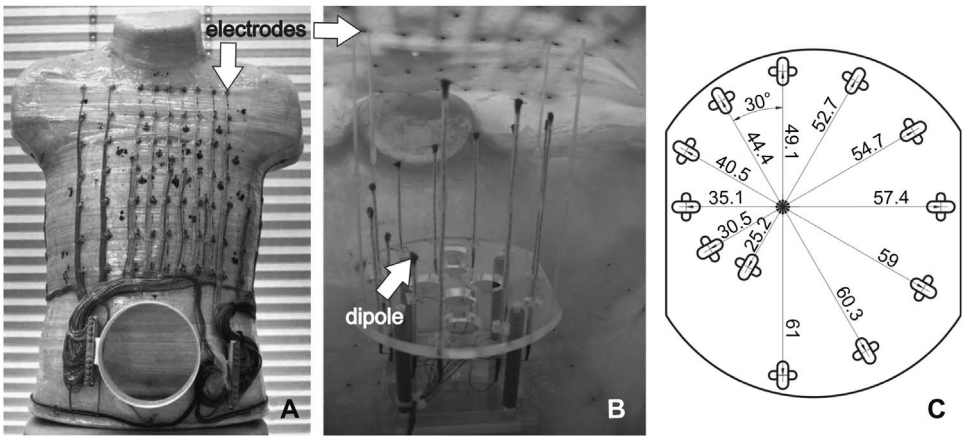

Figure 1 (A) Front view of the physical torso phantom with a total of 138 electrodes, 63 of which are integrated into the anterior chest wall. The opening in the lower part of the torso allows the dipole setups to be mounted inside the torso and the phantom to be filled with NaCl solution. (B) Photograph of an inside view of the torso phantom with the dipole setup of the spatially extended spiral source mounted on the back of the torso (the anterior chest wall with some Ag/AgCl electrodes is visible at the top of the photograph). (C) Graph of the base plate of the dipole setup indicating the distances of the dipole positions from the central point, the angle between the dipoles, and the orientation of the dipoles.

the distances of the dipoles from the center of each setup. The spatially extended spiral was derived from the planar spiral by changing the height of the dipoles above the base plate (Figure 1C). The difference in the dipole heights was 8.2 mm, resulting in a total height of 90.2 mm. This configuration qualitatively mimics a spirally shaped muscle fiber around the cardiac ventricles. Dipole 6 of the spatially extended spiral was at the same height above the base plate as all the dipoles of the planar spiral. The single dipoles were made of platinum, with a length of 10 ± 0.5 mm. Figure 2 shows the arrangement of the dipoles for both configurations, in an opened conformation. Both spiral setups were fixed on the back of the torso with the help of a fastening. Thus, the main axis of the spiral is upwards in Figure 1B, towards the front of the torso. The feed lines for all the dipoles were made from twisted copper wire. The dipole endings were fixed with resin to a glass capillary, in which the twisted copper wires ran to the base plate (Figure 1B, C). For the spatially extended spiral, the dipole endings were adjusted so that they pointed approximately to the position of the next dipole. This led to a gradual tilt in the dipole orientation with respect to the planar spiral, from approximately 15° for the uppermost dipole to 32° for the lower most dipole (Figure 2). The angular spacing between all the dipoles was 30° (Figure 1C), which led to a non-equidistant dipole spacing when plotted in a row (Figure 2). The positions of the dipole tips were digitized (Isotrack II, Polhemus Inc., Colchester, VT, USA) with reference to the mounting rack and transformed into the coordinate system of the torso. The dipoles were fed with a constant current from a power supply with 12 galvanically separated channels. During all measurements, a sinusoidal current of 0.5 mA with a frequency of 20 Hz was applied for each dipole. The dipoles were switched on one by one, starting from a single dipole, until all 12 dipoles were enabled (Figure 3). With these different arrangements, we were able to examine the progression of the electric and magnetic signal strengths for an increasingly spirally shaped current.

Measurements and data analysis

The measurements were made in a magnetically shielded room (AtB SrL, Pescara, Italy) using an ARGOS 200 vector-biomagnetometer (AtB SrL) and an ECG system (AtB SrL). Only the 63 ECG channels on the anterior chest wall were recorded. The electrodes were arranged according to the NEMY standard (non-invasive evaluation of the myocardium) [9]. All of the 195 superconducting quantum interference devices (SQUIDs) of the vector-biomagnetometer were used for the recordings. The sensors were arranged in triplets and distributed over four levels. The lowest level (the main measurement plane) was a planar sensor array consisting of 56 sensor triplets laid out on a hexagonal grid, covering a circular planar surface with a diameter of approximately 25 cm. Only the sensors in the lower plane were considered. The B_z component was used for the analysis because most biomagnetometers only record this component. This resulted in 56 values for each measurement. The intrinsic noise level of the SQUIDs was below 5 $fT/Hz^{-1/2}$ at 10 Hz. The electric and magnetic signals were recorded simultaneously with a sampling rate of 1025 Hz. The patient positioning unit of the Argos 200 (three marker coils, placed on the torso phantom) and the electrodes were digitized. Therefore, the positions of all the sensors were computed in the co-ordinate system of the torso phantom. Figure 4 shows the sensor setup and the torso model based on segmented computed tomography (CT) data.

The raw data were filtered with a 10–35 Hz Butterworth band pass filter. In the channel showing the maximum magnetic amplitude, the time instant of the positive peak amplitude was determined in 20 consecutive artefact-free periods of the sinusoidal signal. Thereafter, for the magnetic channel

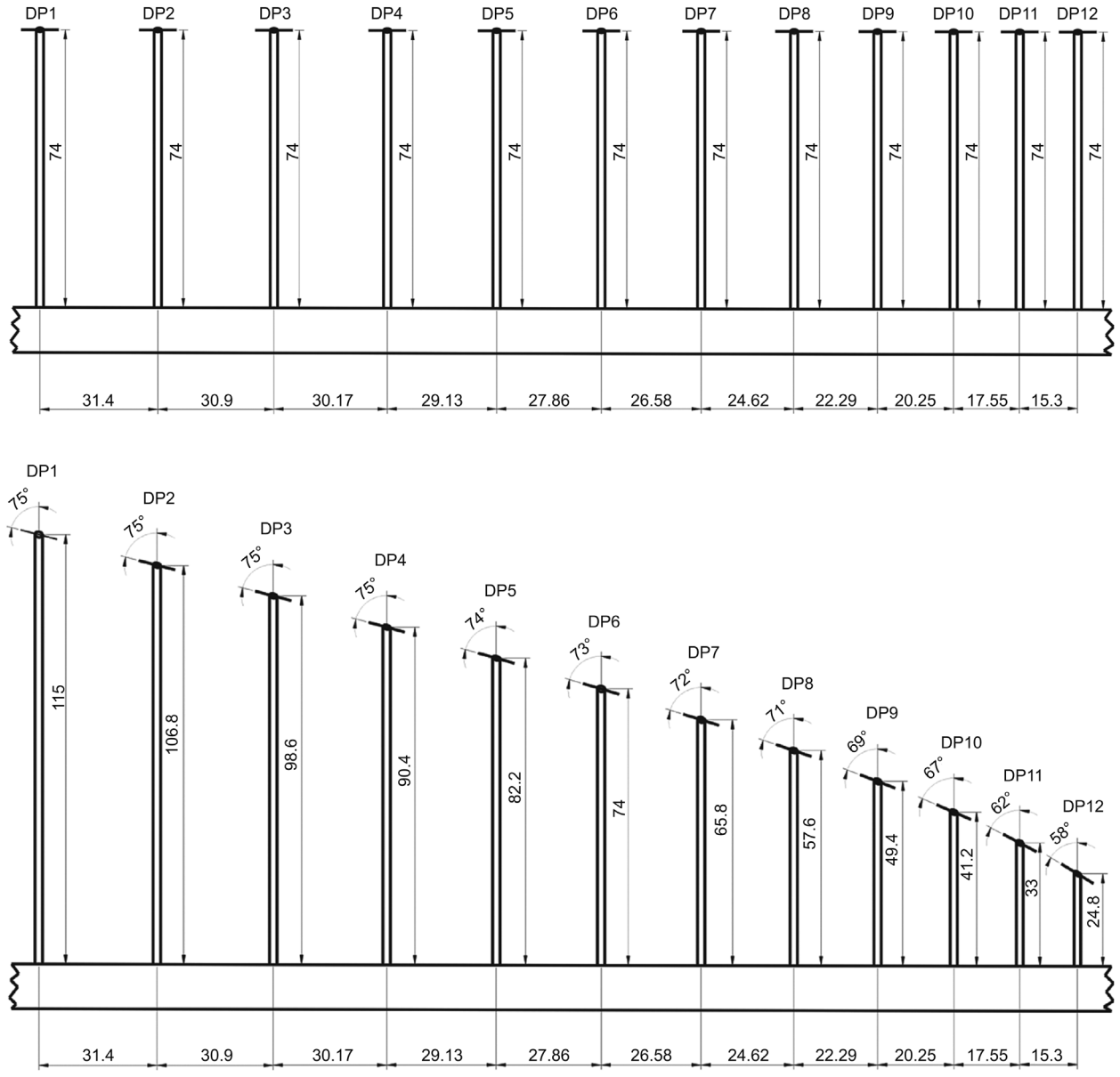

Figure 2 Planar (top) and spatially extended spirals (bottom) in an opened view to demonstrate the different dipole distances, heights above the base plate, and orientations.

and the electric channel that showed the maximum signal amplitudes, the mean values and the standard deviations of the signal strengths were computed over these 20 instants in time. Note that the magnetic and electric signals were in phase. Normalization was applied to make the electric and

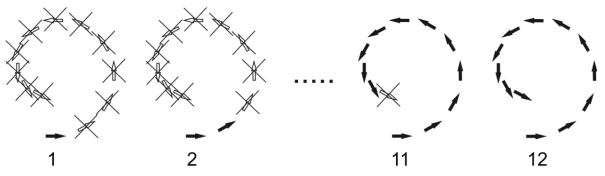

Figure 3 The dipoles of the spiral arrangements are switched on one by one.

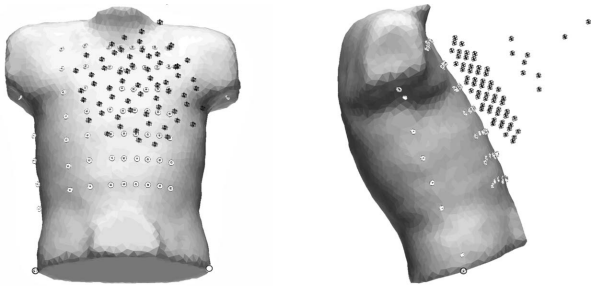

Figure 4 Front view and right side view of the torso phantom model with the positions of the electrodes (white disks) and the positions of the vectorial magnetic sensors (squares and crosses above the torso).

magnetic signal strengths comparable. All values were normalized to the value when one dipole was enabled to allow a comparison to be made with the simplest source model.

Results

Figure 5 shows the measured electric potential and magnetic field maps for both source configurations. For the planar spiral, the electric potential map for one enabled dipole shows the clearly dipolar structure of a source oriented tangentially to the anterior chest wall. With increasing numbers of sources, the zero line becomes more tilted, indicating the vectorial sum of the enabled dipoles. The potential pattern with six enabled dipoles shows the highest amplitude and an almost perpendicular zero line compared with that produced with one enabled dipole. When all 12 dipoles were enabled (complete spiral), we observed a more complex structure in the potential pattern, which faintly shows the underlying spiral. The amplitude of the magnetometer signal increased as the number of enabled dipoles increased. The isocontour plots of the semi-spiral and the complete spiral currents look very similar in the magnetic field patterns, which is partly attributable to the fact that only one maximum is visible.

For the spatially extended spiral, the electric potential map with one enabled dipole shows a pattern with a somewhat radially oriented source, which is caused by the tilt of the dipole (see Methods). This effect is indicated by the greater number of negative isocontour lines compared with the number of positive lines and is, in principal, visible for all potential maps shown in the third row of Figure 5. The magnetic isocontour plots of the spatially extended spiral are qualitatively very similar to the isocontour plots of the planar spiral,

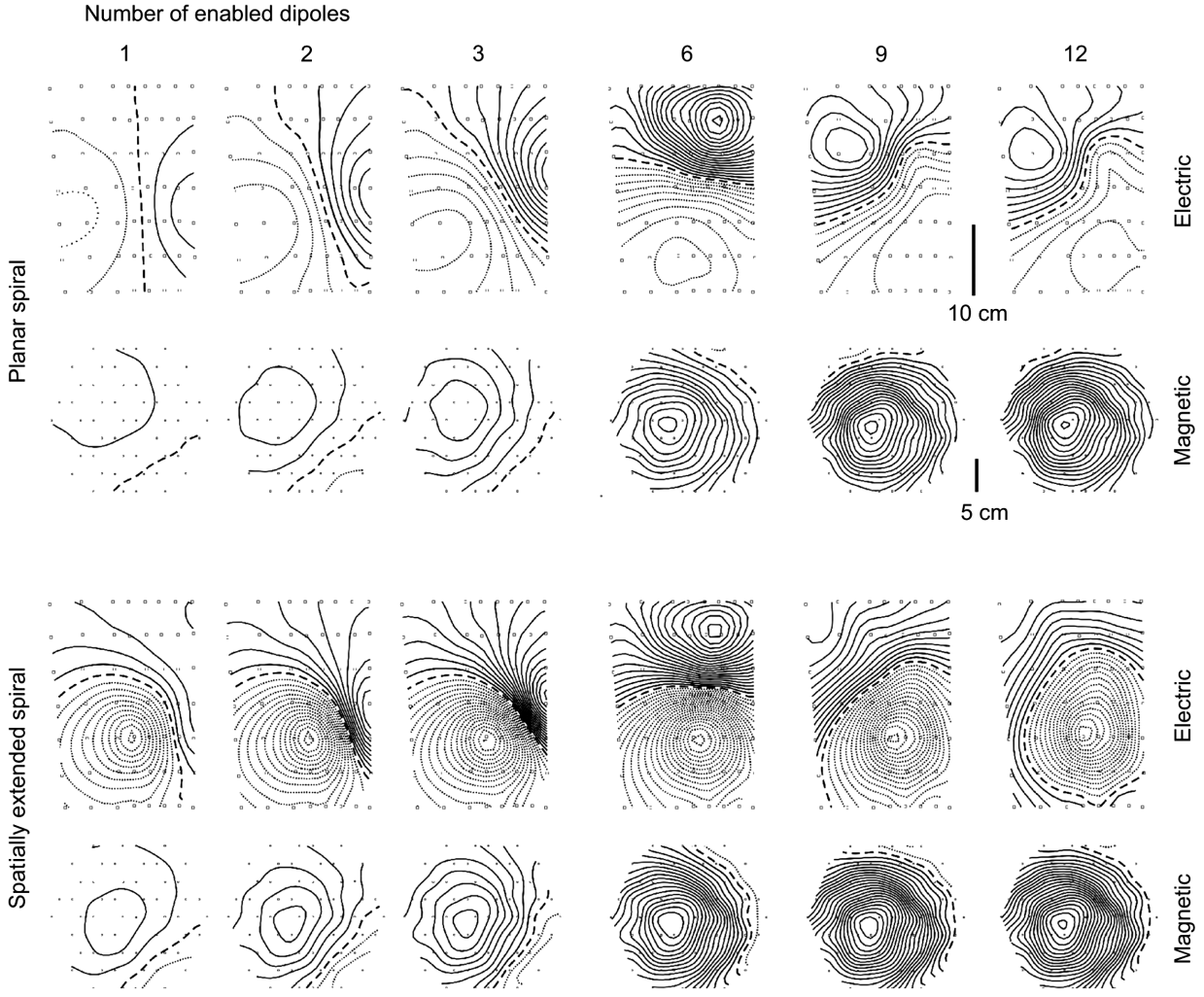

Figure 5 The measured isocontour plots of the electric potentials (first row) and magnetic fields (second row) for the planar spiral and the electric potentials (third row) and magnetic fields (fourth row) for the spatially extended spiral. The number of enabled dipoles is indicated above each column. The contour line increments are 5 pT for the magnetic fields and 0.5 mV for the electric potentials. Solid lines indicate positive values, dotted lines indicate negative values, and the dashed line represents the zero line. The sensor positions are indicated by the small gray squares.

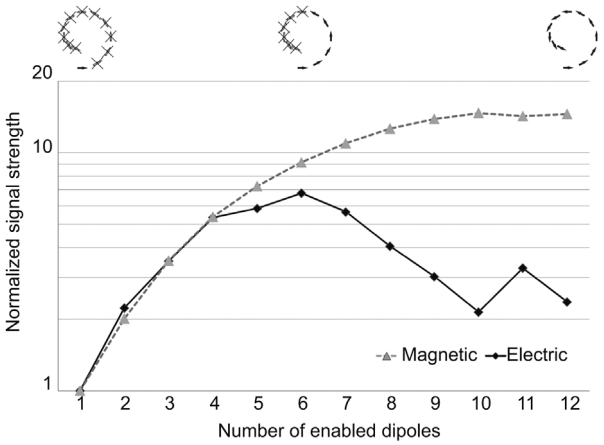

Figure 6 Normalized signal strengths of the electrically and magnetically recorded signals over the number of enabled dipoles for the planar spiral source configuration. The corresponding dipole arrangement is shown at the top.

which would make it difficult to distinguish the two source configurations, i.e., in a source localization scheme.

The normalized amplitudes of the electric and magnetic signals over the number of active dipoles for the planar spiral are shown in Figure 6. As the number of enabled dipoles increases, the spiral shape also becomes more complete. The electric signal strength increases with up to six active dipoles, which represent a semi-spiral (similar to a semicircle), and with up to four dipoles, the increase is similar to the increase in the magnetic signal strength. Thereafter, the electric signal strength decreases almost linearly as the number of enabled dipoles increases up to 10, to a value less than that observed with two active dipoles. For the full spiral, the electric signal strength is also similar to the value produced with two active dipoles. On the contrary, the magnetic signal strength increases with an almost linear slope with up to 10 active dipoles. Thereafter, the signal strength stays approximately constant up to the full spiral. This comparison of the electric and magnetic signal strengths shows that with up to four dipoles, similar behaviors are observed, whereas with increasing numbers of enabled dipoles, a clear dissociation between the two modalities is seen.

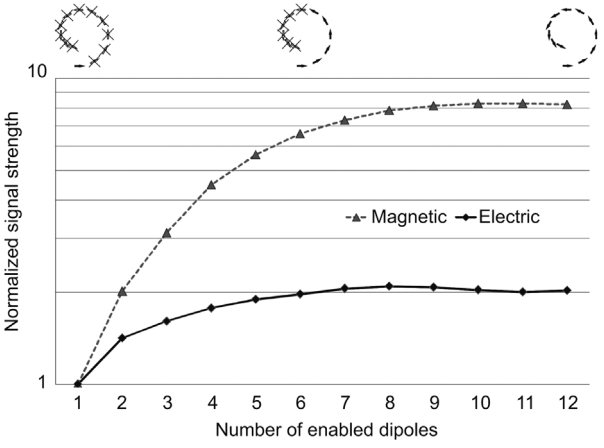

Figure 7 Normalized signal strengths of the electrically and magnetically recorded signals over the number of enabled dipoles for the spatially extended spiral source configuration. The corresponding dipole arrangement is shown at the top.

Figure 7 shows the normalized amplitudes of the electric and magnetic signal strengths over the number of active dipoles for the spatially extended spiral source setup. The electric signal amplitude increases with up to eight active dipoles and decreases slightly starting with the ninth active dipole. The value for the full spiral is less than the value with seven active dipoles. The variation in the signal strength between seven active dipoles and the full spiral is $<5\%$. The amplitude of the magnetic signal increases with up to 10 active dipoles and stays approximately constant thereafter. A comparison of the electric and magnetic signal strengths shows that the magnetic amplitudes increase more than the electric amplitudes.

In both Figures 6 and 7, all the standard deviations are below 0.1% (not shown).

Discussion

We modeled two spirally shaped open loop current distributions with a set of 12 single dipoles in a physical torso phantom. We found that the spirally shaped currents had highly differential effects on the electric and magnetic signal strengths. The differential effect was qualitatively more pronounced for the planar setup than for the spatially extended setup.

We observed a plateau in the magnetic signal strengths when there were a greater number of active dipoles. This plateau was somewhat more pronounced for the spatially extended spiral. The plateau for both configurations can be explained by the increasing symmetry of the dipole arrangement, and a similar finding has been reported previously for an active closed loop current [14]. The explanation for the plateau is based on the same argumentation as in [14]. The more pronounced plateau for the spatially extended spiral is probably attributable to the increasing dipole–sensor distance with increasing numbers of dipoles, which means less amplitude contribution to the total field. Note that, in general, the results for the planar spiral are well comparable to [14] because the heights of the dipoles above the base plates and also above the base plate mountings were similar, resulting in similar source–sensor distances. The decreasing electric signal strength clearly shows the effect on electric signals of getting close to a closed loop.

Similar to the active closed loop circular arrangement in [14], the reduction began when the dipole arrangement exceeded a semi-spiral. Unlike the fully closed loop current in [14], where no significant potential pattern was observable, the full spiral still exhibited a significant electric potential amplitude and a systematic potential pattern. Compared with the experimental results for passive vortex currents in [5], the influence on the electric signal strength was also reduced for the spirally shaped open loop current distribu-

tions in this study. While both passive and active vortex currents might be important in the early diagnosis of myocardial infarction [5, 14], spiral like currents might also account for the experimentally observed differences in healthy volunteers [4, 19].

Comparison of the planar and spatially extended spirals showed the difference in the electric potential distributions most clearly. Because of the more tilted orientation of the dipoles in the spatially extended spiral and their closer proximity to the sensors, a higher amplitude value was already apparent with one enabled dipole (cf. Figure 5, rows 1 and 3). This more tilted orientation led to a stronger radial contribution, where ''radial'' is defined with respect to the anterior chest wall (a dipole pointing towards the chest wall is considered radial and a dipole pointing perpendicular to the chest wall is considered tangential). The reduction in the amplitude of the spatially extended spiral after the ninth dipole had been enabled was considerably less pronounced than that of the planar spiral. This effect can be explained by the spatial extents involved; a much larger radial component existed because of the height difference between the first and last dipoles. The amplitude of the magnetic field was also higher with one enabled dipole for the spatially extended spiral compared with the planar spiral. This can only be attributed to the closer proximity to the sensors. This effect prevailed up to the configuration in which all the dipoles were enabled (cf. Figure 5, rows 2 and 4).

Our experimental results confirm the theoretical predictions of [10]. They predict that a helix-like anatomic structure and spiral-like conductivity profiles can yield electrically silent magnetic fields. Our impressed currents were arranged in a spiral-like manner and showed the dissociation of the magnetic field and electric potential patterns, as well as their signal strengths. Our results are also consistent with a simulation study by Kosch and colleagues [11], who suggested that curved currents (e.g., semi-circles) can already lead to differential effects in the magnetic field and electric potential distributions.

Sensitivity studies of EEG/MEG have been performed [1, 7, 8], similar to investigations of ECG/MCG. These studies have shown that the two modalities are differentially sensitive to sources in certain brain areas and to certain source orientations. Source orientation has been also discussed as an additional possible explanation of the differences in ECG and MCG (e.g., [13]). This influence was not explicitly addressed in our study.

Like the experimental findings in healthy volunteers during exercise [4, 19], we found similar monopolar field patterns in our measurements of full spiral setups. The authors of [4] and [19] argue that closed loop vortex currents could cause the differences they found in ECG and MCG. Our results provide an alternative explanation based on open loop spirally shaped currents.

We have not shown the results for the source localization in the various source configurations. Similar to [20] and [22], we found a source localization accuracy of about 3–5 mm for the single dipoles.

A limitation of our study is in the coverage of the magnetometer. Although the cryostat of the Argos 200 system has a fairly standard diameter compared with those of other flat bottom Dewars, it is obvious from the isocontour plots in Figure 5 that this is not sufficient for the source configurations under consideration, because only one maximum of the distribution is covered. Novel magnetometer approaches to magnetocardiography might overcome this limitation (e.g., [3]).

Conclusion

Our study provides quantitative data supporting the differential influence of spirally shaped open loop currents on magnetocardiographic and electrocardiographic recordings. Such open loop currents may explain, at least in part, the experimentally observed differences between magnetocardiographic and electrocardiographic recordings. Combined bioelectric and biomagnetic measurements provide greater insight into heart activity than do single modality measurements.

Acknowledgements

This work was supported in part by the Deutsche Forschungsgemeinschaft (DFG Grant Ha 2899/7/8-1) and by Bundesministerium für Bildung und Forschung (BMBF Grant 03IP605).

References

[1] Ahlfors SP, Han J, Belliveau JW, Hamalainen MS. Sensitivity of MEG and EEG to source orientation. Brain Topogr 2010; 23: 227–232.
[2] Barach JP. A simulation of cardiac action currents having curl. IEEE T Bio-Med Eng 1993; 40: 49–58.
[3] Bison G, Wynands R, Weis A. Dynamical mapping of the human cardiomagnetic field with a room-temperature, laser-optical sensor. Opt Express 2003; 11: 904–909.
[4] Brockmeier K, Schmitz L, Chavez JB, et al. Magnetocardiography and 32-lead potential mapping: repolarization in normal subjects during pharmacologically induced stress. J Cardiovasc Electrophysiol 1997; 8: 615–626.
[5] Dutz S, Bellemann ME, Leder U, Haueisen J. Passive vortex currents in magneto- and electrocardiography: comparison of magnetic and electric signal strengths. Phys Med Biol 2006; 51: 145–151.
[6] Geddes LA, Baker LE. Specific resistance of biological material-a compendum of data for biomedical engineer and physiologist. Med Biol Eng 1967; 5: 271–293.
[7] Goldenholz DM, Ahlfors SP, Hamalainen MS, et al. Mapping the signal-to-noise-ratios of cortical sources in magnetoencephalography and electroencephalography. Hum Brain Mapp 2009; 30: 1077–1086.
[8] Haueisen J. Tangential and radial epileptic spike activity: different sensitivity in EEG and MEG. J Clin Neurophysiol 2010; 27: 67.
[9] Hoekema R, Huiskamp GJM, Oostendorp TF, Uijen GJH, Vanoosterom A. Lead system transformation for pooling of

body-surface map data – a surface laplacian approach. J Electrocardiol 1995; 28: 344–345.
[10] Irimia A, Swinney KR, Wikswo JP. Partial independence of bioelectric and biomagnetic fields and its implications for encephalography and cardiography. Phys Rev E 2009; 79 (5 Pt 1): 051908.
[11] Kosch O, Meindl P, Steinhoff U, Trahms L. Physical aspects of cardiac magnetic fields and electric potentials. In: Nenonen J, Katila T, editors. Biomag 2000, Proc. 12th Int Conf on Biomagnet Helsinki University of Technology, Espoo, Finland, 2001. p 553–556.
[12] Kwon H, Kim K, Lee YH, et al. Non-invasive magnetocardiography for the early diagnosis of coronary artery disease in patients presenting with acute chest pain. Circ J 2010; 74: 1424–1430.
[13] Lant J, Stroink G, Tenvoorde B, Horacek BM, Montague TJ. Complementary nature of electrocardiographic and magnetocardiographic data in patients with ischemic-heart-disease. J Electrocardiol 1990; 23: 315–322.
[14] Liehr M, Haueisen J, Goernig M, Seidel P, Nenonen J, Katila T. Vortex shaped current sources in a physical torso phantom. Ann Biomed Eng 2005; 33: 240–247.
[15] On K, Watanabe S, Yamada S, et al. Integral value of JT interval in magnetocardiography is sensitive to coronary stenosis and improves soon after coronary revascularization. Circ J 2007; 71: 1586–1592.
[16] Park JW, Leithauser B, Vrsansky M, Jung F. Dobutamine stress magnetocardiography for the detection of significant coronary artery stenoses – A prospective study in comparison with simultaneous 12-lead electrocardiography. Clin Hemorheol Microcirc 2008; 39: 21–32.
[17] Roth BJ, Wikswo JP. Electrically silent magnetic-fields. Biophys J 1986; 50: 739–745.
[18] Sander TH, Knosche TR, Schlogl A, et al. Recent advances in modeling and analysis of bioelectric and biomagnetic sources. Biomed Tech 2010; 55: 65–76.
[19] Takala P, Hanninen H, Montonen J, et al. Magnetocardiographic and electrocardiographic exercise mapping in healthy subjects. Ann Biomed Eng 2001; 29: 501–509.
[20] Tenner U, Haueisen J, Nowak H, Leder U, Brauer H. Source localization in an inhomogeneous physical thorax phantom. Phys Med Biol 1999; 44: 1969–1981.
[21] Tolstrup K, Madsen BE, Ruiz JA, et al. Non-invasive resting magnetocardiographic imaging for the rapid detection of ischemia in subjects presenting with chest pain. Cardiology 2006; 106: 270–276.
[22] Wetterling F, Liehr M, Schimpf P, Liu H, Haueisen J. The localization of focal heart activity via body surface potential measurements: tests in a heterogeneous torso phantom. Phys Med Biol 2009; 54: 5395–5409.
[23] Wikswo JP, Barach JP. Possible sources of new information in the magnetocardiogram. J Theor Biol 1982; 95: 721–729.

Received March 21, 2011; accepted July 21, 2011